Powder Technology 386 (2021) 144–153

Contents lists available at ScienceDirect

Powder Technology

journal homepage: www.elsevier.com/locate/powtec

Discrete element modelling of track ballast capturing the true shape of ballast stones

Jacob Mortensen [a], Joachim Faldt Faurholt [a], Emil Hovad [b], Jens Honoré Walther [a,c,*]

[a] DTU Mechnical Engineering, Technical University of Denmark, Nils Koppels Allé. Building 403, room 110, 2800 Kgs. Lyngby, Denmark
[b] DTU Compute, Technical University of Denmark, Technical University of Denmark, Richard Petersens Plads. Building 324, 2800 Kgs. Lyngby., Denmark
[c] Computational Science and Engineering Laboratory, ETH, Zürich CH-8092, Switzerland

ARTICLE INFO

Article history:
Received 22 May 2020
Received in revised form 3 February 2021
Accepted 22 February 2021
Available online 13 March 2021

Keywords:
Discrete element method
Track ballast modelling
Particle shape modelling
3D scanning

ABSTRACT

Railway ballast affected by heavy cyclic loading degrades and spreads resulting in an uncomfortable transportation caused by undesirable vibrations. Restoring a well sorted track ballast can be expensive. This paper analyzes track ballast deformation using the Discrete Element Method (DEM). The simulations are performed using the STAR-CCM+ software in a three-dimensional domain. Four track ballast models are studied. The first two models describe the ballast as spheres with and without rolling resistance, respectively. The third model uses a clump model that allows breaking of the ballast, whereas the fourth model describes the ballast as composite particles generated from 3D-scanned ballast stones. The sleepers and rails are modelled as DEM particles. As a supplement to the study of different ballast models, the influence of variation in the loading profile is investigated. The largest obtained deformation is observed in the ballast modelled as spheres and the smallest deformation in the ballast modelled from the 3D scanned ballast stones. The results highlight the importance of describing the ballast as non-spherical geometries.

1. Introduction

The traditional track structure consists of three components: rails, sleepers and track ballast. The sleepers are partially submerged in crushed granite stones. A collection of stones is known as ballast and after heavy cyclic loading the ballast degrades, densifies and spreads resulting in poor stability, which leads to uneven transportation. The most common rail failures are caused by degradation mechanisms such as wear, plastic flow, and rolling contact fatigue [1–3]. The ballast deformation can be analyzed numerically using the Discrete Element Method (DEM). The tendency of trains reaching higher velocities causes greater maintenance expenses, therefore new ballast types and different ballast stone shapes are considered. Achieving realistic, accurate simulations of the track ballast deformation is desirable since new ballast types or stone shapes can be studied with few difficulties. DEM is an effective method for computing interactions between particles and motions of particles. In this study the ballast is simulated using the commercial software STAR-CCM+ which bases its DEM on the theory described by Cundall and Strack [4] along with the Hertz-Mindlin contact model described by Di Renzo and Di Maio [5], and the particle bonding model by Potyondy and Cundall [6]. In this study the ballast deformation is simulated in a three-dimensional domain using four different ballast methods with a simulation procedure inspired by the work of Lobo-Guerrero and Vallejo [7], and Mahmouda and Papagiannakisb [8]. The focus of the present study is the capturing of the real geometry of the ballast stones and sleepers, and to compare the complex ballast model with more simple models, used in the literature. Accordingly, the ballast is modelled from actual 3D-scanned stones delivered by Banedanmark, which are assembled into unbreakable clumps, with sleepers modelled as DEM particles. This method is compared to other ballast models. One is modelled as spheres with and without rolling resistance, and another as DEM particles assembled into breakable clumps. In this research the sphere shaped ballast is used as benchmark to compare the results with other similar studies such as [8]. The clumps and 3D shaped stones fulfills the specifications for ballast stones described by Banedanmark [9]. Banedanmark is responsible for maintenance and traffic control on the Danish railway network. In the simulations the sleepers and rails are described as single polyhedral DEM particles. In addition to the study of the described ballast types the impact of different load functions are tested.

Previous research of ballast deformation and degradation includes the work of Feng et al. [10] and Romero et al. [11] who described common defects such as worn and missing fasteners. Zakeri and Rezvani [12] presented a thorough analysis of the most common defects of sleepers during production, transportation, and operation. Within

* Corresponding author at: DTU Mechnical Engineering, Technical University of Denmark, Nils Koppels Allé. Building 403, room 110, 2800 Kgs. Lyngby, Denmark.
E-mail addresses: s164321@student.dtu.dk (J. Mortensen), s164390@student.dtu.dk (J.F. Faurholt), emilh@dtu.dk (E. Hovad), jhw@mek.dtu.dk (J.H. Walther).

https://doi.org/10.1016/j.powtec.2021.02.066
0032-5910/

operation and maintenance periods, bending cracks, sleeper breakage due to derailments and cutting cracks are the most usual defects in sleepers. Ballast layer is a track element that plays an important role in the overall track degradation process. Degradation phenomena in this layer are properly reported in [13–16]. The breakage behaviour of ballast stones made of different samples has been studied by Tutumluer and Hashash [17] using DEM along with laboratory ballast materials tests. They found that the breakage behaviour differs considerably when using fouled and clean ballast. Furthermore the loading profiles from different train velocities are considered in this research. Another study investigating the track ballast deformation behaviour during cyclic loading, is a study conducted by Lobo-Guerrero and Vallejo [7]. In this study the ballast is simulated using two approaches. One of them uncrushable while the other crushable. The study showed greater vertical deformations in the crushable ballast than the uncrushable ballast. Ballast deformation simulations using DEM in a two-dimensional domain was also studied by Mahmouda and Papagiannakisb [8]. Here the effect of aggregates particle shapes on the deformation was studied with the allowance of breakage. The study showed promising results using aggregate shapes rather than sphere-shaped ballast stones. Dahal and Mishra [18] simulated ballast particle breakage by calibrating the crushing criteria in the DEM simulation by particle crushing laboratory test. Polyhedral ballast shapes were compared with spherical shaped ballast stones. Commonly the literature states that shape and breakage are essentials when simulating track ballast behaviour using DEM. In the literature numerous approaches have been used to represent ballast for cyclic loading simulations. Abundant research have investigated on sphere shaped ballast, both [7,8] focuses their studies on sphere shaped ballast with the allowance of breakage in 2D domains. Also quite a number of studies have investigated non-spherical ballast in 3D domains. Tutumluer and Hashash [17], represented the ballast as 3D Polyhedrons, using 3D- scannings of lime-stone, obtaining realistic shaped ballast. Dahal and Mishra [18] used a ballast model similar to the "3D - scanned ballast" model presented in this study, where overlapping spheres represents the ballast stone, here 3 real stones were scanned and modelled by overlapping spheres. Another study representing ballast stones by overlapping spheres is the study conducted Zhou et al. [19], here the main interest was to simulate the tamping procedure. The present study is focused on modelling of realistic ballast stones interacting with the sleepers in three dimensions and subjected to cyclic load.

2. Discrete element method theory

Simulations using the Discrete Element Method (DEM) are conducted in the present study using the commercial software STAR-CCM +. Discrete element modelling is based on Newton's second law.

$$\vec{F}_i = m_i \vec{a}_i, \tag{1}$$

where $\vec{F}_i$, m_i, and $\vec{a}_i$ denote the force, mass and corresponding acceleration of the i-th particle. The forces on all particles are calculated according to the described theory for each time step. For each time step the particles are assigned a position, velocity, angular velocity, and orientation based on the previous time step.

2.1. Governing equations

The description of the DEM theory is based on [20–22]. The total force on a particle i in a time step is calculated by summing the forces from all the contributions from the particles interaction with particle j

$$\vec{F}_i^{tot} = \vec{F}_u + m_i \vec{g} + \sum_j \left(\vec{F}_{n_{ij}} + \vec{F}_{t_{ij}}\right), \tag{2}$$

where $\vec{g}$ denotes the acceleration due to gravity, and $\vec{F}_u$ an external body force which is used to impose the cyclic loading of the rails. $\vec{F}_{n_{ij}}$ and $\vec{F}_{t_{ij}}$ denotes the force normal and tangential to a contact plane between particle i and j respectively. The total torque on particle i is

$$\vec{T}_i^{tot} = -R_i \sum_j \vec{n}_{ij} \times \vec{F}_{t_{ij}} + \vec{T}_{roll_{ij}}, \tag{3}$$

where R_i is the radius of the i-th particle, and $\vec{n}_{ij}$ denotes the normal to the contact plane. $\vec{F}_{n_{ij}}$ and $\vec{F}_{t_{ij}}$ are obtained from the applied contact model. In this study two contact models are used, the Hertz-Mindlin and the linear spring model. The unique theory for each contact model is described in Sections 2.2 and 2.3. $\vec{T}_{roll_{ij}}$ is the rolling resistance which is modelled using the constant torque method. The torque is given as:

$$\vec{T}_{roll_{ij}} = -\frac{\omega_{ij}}{|\omega_{ij}|_2} \mu_r R_{eq} \left|\vec{F}_{n_{ij}}\right|_2, \tag{4}$$

where μ_r is the coefficient of rolling resistance, ω_{ij} is the relative angular velocity between the two particle $\omega_{ij} = \omega_i - \omega_j$, and R_{eq} is the relative radius of particles i and j

$$R_{eq} = \left(\frac{1}{R_i} + \frac{1}{R_j}\right)^{-1}. \tag{5}$$

The constant torque method is used in one simulation where complex shape of the ballast is modelled as simple spheres. The model is added to make up for the fact that complex shapes contributes to the restraining of rolling. The overlap normal to the contact plane between particle i and j is calculated based on following equation:

$$\delta_{n_{ij}} = (R_i + R_j) - r_{ij}, \tag{6}$$

where $\vec{r}_{ij}$ denotes the distance vector between particle center of particle i and j and $r_{ij} = \left|\vec{r}_{ij}\right|_2$. The relative normal velocity and relative tangential velocity between particle i and j are respectively given as:

$$\vec{v}_{n_{ij}} = \left(\vec{v}_{ij} \cdot \vec{n}_{ij}\right) \vec{n}_{ij}, \tag{7}$$

$$\vec{v}_{t_{ij}} = \vec{v}_{ij} - \vec{v}_{n_{ij}} - \left(\vec{\omega}_i R_i + \vec{\omega}_j R_j\right) \times \vec{n}_{ij}, \tag{8}$$

$\vec{v}_{ij} = \vec{v}_i - \vec{v}_j$ is the relative velocity between particle i and j. The tangential displacement vector is $\vec{t}_{ij} = \vec{v}_{ij} \Delta t$ with Δt being the time step. The tangential displacement is defined as $\delta_{t_{ij}} = \left|\vec{t}_{ij}\right|_2$. The normal force is defined as:

$$\vec{F}_{n_{ij}} = -K_n \delta_{n_{ij}} \vec{n}_{n_{ij}} - N_n \vec{v}_{n_{ij}}, \tag{9}$$

K_n is the normal spring stiffness, and N_n is the normal damping. How these parameters are calculated differs between the Hertz-Mindlin and the linear spring model. When $|K_t \delta_{t_{ij}}| < |K_n \delta_{n_{ij}}| C_{fs}$, with C_{fs} being the static friction coefficient, the tangential force is defined as:

$$\vec{F}_{t_{ij}} = -K_t \frac{\vec{t}_{ij}}{\left|\vec{t}_{ij}\right|_2} \delta_{t_{ij}} - N_t \vec{v}_{t_{ij}} + \vec{T}_{roll_{ij}}, \tag{10}$$

otherwise the tangential force is defined as:

$$\vec{F}_{t_{ij}} = \frac{\left|K_n \delta_{n_{ij}}\right|_2 C_{fs} \vec{t}_{ij}}{\left|\vec{t}_{ij}\right|_2}, \tag{11}$$

where K_t is the tangential spring stiffness, and N_t the tangential damping. These values differs between the models too.

2.2. Hertz-Mindlin model

The stiffness models used by the Hertz-Mindlin model are defined as

$$K_n = \frac{4}{3} E_{eq} \sqrt{\delta_{n_{ij}} R_{eq}}, \tag{12}$$

$$K_t = 8 G_{eq} \sqrt{\delta_{t_{ij}} R_{eq}}, \tag{13}$$

with

$$E_{eq} = \left(\frac{1-\nu_i^2}{E_i} + \frac{1-\nu_j^2}{E_j} \right)^{-1} \tag{14}$$

being the relative Young's modulus and

$$G_{eq} = \left(\frac{2(2-\nu_i)(1+\nu_i)}{E_i} + \frac{2(2-\nu_j)(1+\nu_j)}{E_j} \right)^{-1} \tag{15}$$

the relative shear modulus between particles i and j. The normal and tangential damping used by Hertz-Mindlin is defined as:

$$N_n = \sqrt{5 K_n M_{eq}} N_{n-damp}, \tag{16}$$

$$N_t = \sqrt{5 K_t M_{eq}} N_{t-damp}, \tag{17}$$

with M_{eq} being the relative mass of particle i and j

$$M_{eq} = \left(\frac{1}{M_i} + \frac{1}{M_j} \right)^{-1}. \tag{18}$$

N_{n-damp} is the normal damping coefficient and N_{t-damp} is the tangential damping coefficient. These are defined as:

$$N_{n-damp} = \frac{-\ln(C_{n,res})}{\sqrt{\pi^2 + \ln(C_{n,res})^2}}, \tag{19}$$

$$N_{t-damp} = \frac{-\ln(C_{t,res})}{\sqrt{\pi^2 + \ln(C_{t,res})^2}}, \tag{20}$$

where $C_{n,res}$ is the coefficient of normal restitution, and $C_{t,res}$ is the coefficient of tangential restitution. The STAR-CCM+ based Hertz-Mindlin contact model requires three parameters. These are the static friction coefficient, the normal, and the tangential coefficient of restitution.

2.3. Linear spring model

The linear spring model defines K_n, K_t, N_n, and N_t differently than the Hertz-Mindling model while the damping coefficients remain the same. For the linear spring model the normal spring constant, K_n, and tangential spring constant, K_t, are set to a constant value. The normal and tangential damping for the linear spring model are defined as:

$$N_n = 2 N_{n-damp} \sqrt{K_n M_{eq}}, \tag{21}$$

$$N_t = 2 N_{t-damp} \sqrt{K_t M_{eq}}. \tag{22}$$

For interactions between a particle and a wall it applies for both models that the wall is modelled to have an infinite radius and an infinite mass. For these interaction $M_{eq} = M_i$ and $R_{eq} = R_i$ for particle i. The linear spring model in STAR-CMM+ requires a total of five parameters. These are the static friction coefficient, the normal and the tangential coefficient of restitution - similar to the Hertz-Mindlin model. Furthermore it requires a normal and a tangential spring stiffness.

2.4. Clumps bonding and breakage model

For the track ballast simulated as clumps a bonding model is required. The bonding of individual particles in a composite particle is rigid and the particles are only treated individually for contact detection. Otherwise the composite particles are treated as single rigid particles. Particles in a particle clump are treated individually with their own velocity, position, angular velocity, and orientation [22].

2.4.1. Bonding model

The bonding model used the bonded-particle model by Potyondy and Cundall [6,22]. Here, the force and torque are calculated as:

$$\vec{F}_i = F_n \vec{n}_i + F_s \vec{t}_i, \tag{23}$$

$$\vec{M}_i = M_n \vec{n}_i + M_s \vec{t}_i, \tag{24}$$

with respect to the contact plane, where F_n and M_n are the normal components of the force and torque. F_s and M_s are the shear/tangential components of the force and torque. The force and moments are computed incrementally cf. [6], thus

$$\Delta F_n = k_n A \Delta U_n, \tag{25}$$

$$\Delta M_n = -k_s J \Delta \Omega_n, \tag{26}$$

$$\Delta F_s = -k_s A \Delta U_s, \tag{27}$$

$$\Delta M_s = -k_n I \Delta \Omega_s, \tag{28}$$

here $A_i = \pi {R_i}^2$, $I_i = \frac{1}{4}\pi {R_i}^4$, $J_i = \frac{1}{2}\pi {R_i}^4$, $k_n = \frac{E}{R_i + R_j}$, and $k_s = 6\left(\frac{G}{R_i + R_j}\right)$. With the relative particle velocity $\vec{v}_{ij}$, and the relative angular velocity $\vec{\omega}_{ij}$, the relative displacements $\Delta\vec{U}_{ij}$ and $\Delta\vec{\Omega}_{ij}$ are computed as:

$$\Delta\vec{U}_{ij} = \vec{v}_{ij} \Delta t, \tag{29}$$

$$\Delta\vec{\Omega}_{ij} = \vec{\omega}_{ij} \Delta t, \tag{30}$$

The ΔU_{ij} and $\Delta\Omega_{ij}$ describe the relative displacements between particle i and j, each having a normal and tangential component denoted $(\Delta U_n, \Delta\Omega_n)$ and $(\Delta U_s, \Delta\Omega_s)$.

2.4.2. Breakage model

In the simulations containing clumps the breakage model “Simple Failure Model” [22] is applied, here the maximum tensile and shear stress of a bonded particle are calculated as:

$$\delta_{max} = -\frac{F_n}{A} + \frac{|M_s| R}{I}, \tag{31}$$

$$\sigma_{max} = \frac{|F_s|}{A} + \frac{|M_n| R}{J}. \tag{32}$$

The model computes a bond to break if:

$$\delta_{max} > \delta_m \tag{33}$$

or

$$\sigma_{max} > \sigma_m \tag{34}$$

In the simulations a constant shear and tensile strength method is used. The tensile and shear strength used in the simulation of the clumps are stated in Section 3.1.2.

3. Simulation procedure

This study investigates the behaviour of realistically shaped ballast stones interacting with discrete sleepers. The ballast is compared with three other simplified ballast models. Furthermore variations in the load function is studied. The simulation of the deformation of the ballast follows the same procedure, except the modelling of the ballast itself. All simulations are computed in a domain with dimensions $(L \times W \times H) = (1.0\,\text{m} \times 2.1\,\text{m} \times 1.5\,\text{m})$ with all outer boundaries set as walls. The computational domain is shown in Fig. 1.

3.1. Track ballast modelling

In the simulations the track ballast is modelled using four different methods: spheres with and without rolling resistance, clumps and 3D scanned stones. The models differ in computational cost and representation of the real situation. All the ballast models are simulated with the mechanical properties stated in Table 1. The non-sphered ballast models used in this study comply with ballast specifications and requirements stated by Banedanmark. Banedanmark suggest that the ballast must be rather cubic, meaning that the length-to-width ratio has to be less than 2, furthermore the length and width of the stones needs to be in a range of 31.5 to 50 mm, however small amounts of bigger and smaller stones are accepted [9].

3.1.1. Spheres (ballast model 1 and 2)

This method is the least representational model. It simulates the ballast as spheres with a diameter of $d = 40\,\text{mm}$. The spheres are simulated without and with rolling resistance denoted ballast model 1 and 2 respectively. In ballast model 2 the rolling resistance coefficient is set to $C_{rr} = 0.5$.

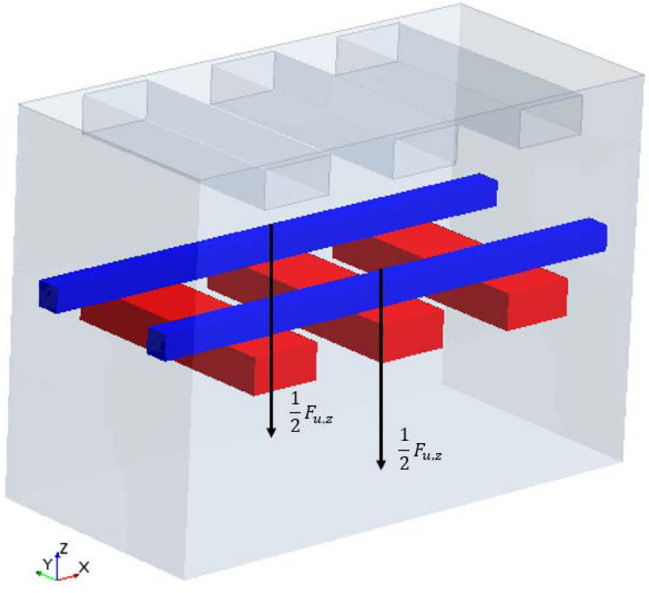

Fig. 1. The computation domain including a free body diagram of the sleepers and cubic rails used in the simulations.

Table 1
Mechanical properties of the ballast, based on granite stone [23]. Here ν denotes the Poisson's ratio, C_n and C_t are the normal- and tangential coefficients of restitution respectively, ρ denotes the density, μ denotes the coefficient of friction, and E the modulus of elasticity.

ν [−]	$C_{n,res}$ [−]	$C_{t,res}$ [−]	ρ [kg/m^3]	μ [−]	E [GPa]
0.1	5×10^{-3}	5×10^{-3}	2700	0.7	60

3.1.2. Clumps (ballast model 3)

The clump approach is a method to obtain more realistically shaped ballast stones. The shape of the clump is the authors proposal, for a stone having a length to width ratio of 1.5, while keeping the number of particles in one clump few, to keep the computational cost low. The clumps are generated from bonding of 10 equally sized spheres and the model is shown in Fig. 2. The size distribution of the clumps are based on the average volume and the standard deviation of the 10 scanned stones assuming a normal distribution. The clumps are breakable with the implementation of the earlier described simple failure model described in Section 2.4.2. The clumps are computed with a tensile and shear strength of $\delta_m = 25$ GPa and $\sigma_m = 40$ GPa. The values are based on [23,24]. Note that this model is simplified from reality since granite has a size and geometry dependent shear and tensile strength. This relationship is discussed by [7].

3.1.3. 3D scanned stones (ballast model 4)

To obtain the possibility to simulate the rough surface and natural geometry of granite stones, 10 actual granite ballast-stones delivered by Banedanmark were 3D-scanned. The scanning procedure can be seen in Fig. 3 for two of the ballast stones. The composite particles were generated from the CAD-files, obtained from the scannings, in a geometry sphere fitting routine. Here a user defined number of overlapping spheres are chosen to fit the geometry of the 3D-scannings, the generated composite particle do not exceed the boundary of the original scan. In ballast model 4, 15 overlapping spheres were chosen to fit the geometry of the scannings. This makes the volume of the STAR-CCM+ generated composite particles lower than the 3D scanned output files. On average the volume of the generated composite particles are 75% of the original volume. The sphericity index of each of the scanned ballast stone is stated in Table 2.

3.2. Injection of the track ballast

The four ballast types are injected in the simulation domain as illustrated in Fig. 4. In order to obtain a randomly mixed ballast section the particles are injected with initial velocity, spacing, and random orientation. Furthermore the DEM-clumps and 3D-scanned stones are injected in one time step to avoid a biased distribution. Each ballast type is injected with a layer height of 0.4 m. After injection the ballast is simulated to fall under the influence of gravity until the summed magnitude velocity of the ballast reaches <1 m/s. At this state the ballast is assumed to be at rest.

3.3. Compression of the track ballast

After the injection the ballast is compressed in order to smooth the distribution of particles, and to avoid interstices in the ballast. The compression is performed using a "ballast compressor" which is modelled as a wall filling the horizontal cross sectional area of the simulation domain. The compressor is moved downwards with a fixed velocity of 10^{-7} m per time step. The compression is first performed on the clumps until the maximum shear or tensile stress reaches the breakage limit of a clump. The reported contact force at this state is afterwards applied to

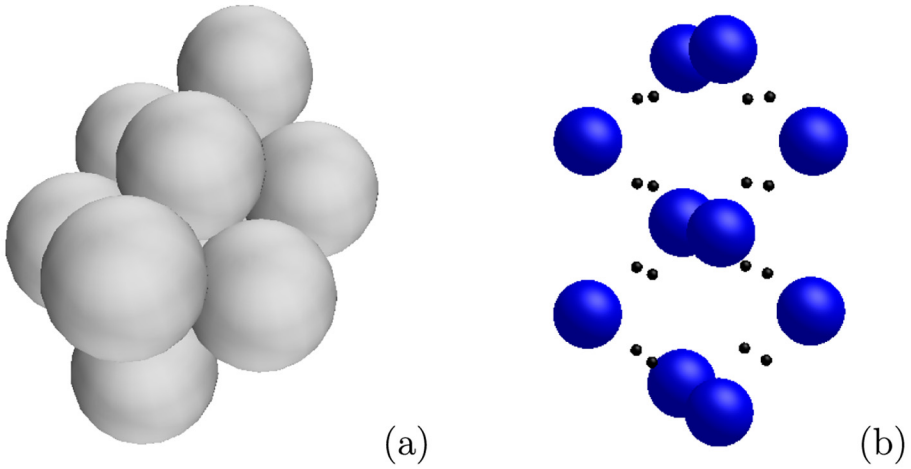

Fig. 2. Clumps (ballast model 3). (a) Model of a clump. (b) model of a clump with the bonds visualised. The bonds are shown in black. The particles are shrunk in order to see the placement of the bonds. The total number of bonds per clump is 19 (16 are visible). The last 3 bonds are placed between each pair of the particles in the middle.

the compression of the spheres and 3D-scanned stones which do not allow breakage).

3.4. Sleeper and load profile modelling

In this study the sleepers are modelled as DEM particles. The dimensions of the sleepers used in the simulation are $(L \times W \times H) = (2.1\,\text{m} \times 0.3\,\text{m} \times 0.15\,\text{m})$. For each simulation 3 sleepers are placed with a distance of 0.3 m. The DEM sleepers are injected as single polyhedral DEM particles after the compression of the ballast. Furthermore, two rails are injected on top of the sleepers, in order to be able to model unevenly distributed load. The dimension of the rails are $(L \times W \times H) = (2.1\,\text{m} \times 0.1\,\text{m} \times 0.1\,\text{m})$. The rails and sleepers are injected at a height of 0.01 m above the highest placed particle. The sleepers and rails fall only under the influence of gravity until the summed magnitude velocity of all particles reaches <1 m/s. The cyclic loading model is computed by adding an external body force on the rails. The cyclic load model is computed as a trigonometric function with a peak of 63 kN and a trough of 1 kN. Similar loading profiles have been used by [7,8] based on [17]. The cyclic loading is modelled using the function

Table 2

Sphericity index of the ballast stones given by $\psi = \frac{\sqrt[3]{36\pi V^2}}{A}$, as suggested in [25]. Here V and A are the volume and surface area for the stone respectively.

No. #	1	2	3	4	5	6	7	8	9	10
ψ	0.711	0.771	0.732	0.689	0.776	0.779	0.795	0.799	0.727	0.772

$$F_{u,z} = \min\left[-\sin\left(\frac{t}{T_c}\pi\right), 0\right] F_{amp}, \tag{35}$$

where t denotes the physical simulation time, T_c is the cycle time for loading, and $F_{amp} = 62\,\text{kN}$ is the amplitude. This formula incorporates a rest time which is equal to the cycle time. Rest time refers to the time between the rails are unloaded until next load. In Fig. 5 this function is applied with a cycle time of 0.05 s.

For simulations without rest time the formula is:

$$F_{u,z} = -\left|\sin\left(\frac{t}{T_c}\pi\right)\right| F_{amp}, \tag{36}$$

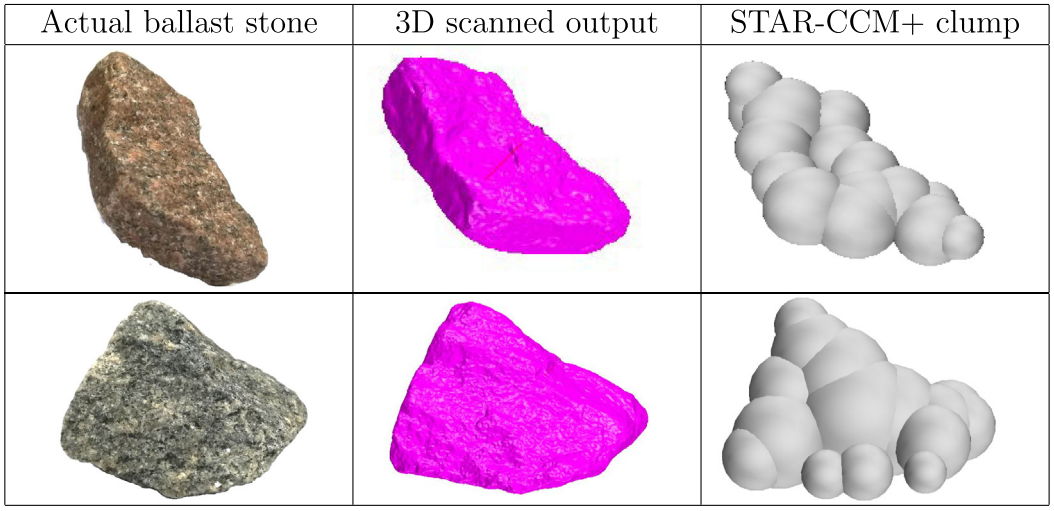

Fig. 3. 3D scanned stones (ballast model 4). Modelling of the 3D-scanned stones, showing a picture of the actual collected ballast stone, the 3D scanned output, and the generated clumps in STAR-CCM+. Corresponding to stone number 1 and 6 in Table 2.

Table 3
Interaction models chosen for the simulations.

Component 1	Component 2	Interaction model	Spring Stiffness [N/m]
Ballast	Ballast	Hertz-Mindlin	–
Ballast	Wall	Hertz-Mindlin	–
Ballast	Sleepers	Linear spring	10^9
Sleepers	Rails	Linear spring	10^9

For simulations with rest time longer than the cycle time multiples of the cycle time with high numerical value are added to Eq. (35) in order to cancel out the desired number of cycles before next load. The formula used for 0.15 s of rest time is:

$$F_{u,z} = \min\left[-\sin\left(\frac{t}{T_c}\pi\right) + \max\left[-200\sin\left(\frac{t}{2T_c}\pi\right), 0\right], 0\right] F_{amp}. \quad (37)$$

For 0.35 s of rest time the formula is:

$$F_{u,z} = \min[-\sin\left(\frac{t}{T_c}\pi\right) + \max\left[-200\sin\left(\frac{t}{2T_c}\pi\right), 0\right] + \max\left[-400\sin\left(\frac{t}{4T_c}\pi\right), 0\right], 0] F_{amp} \quad (38)$$

3.5. Interactions models

The interaction of the walls and the DEM particles are modelled with Hertz-Mindlin and the linear spring model along with the physics described in Section 2. The interaction models used on the different components are stated in Table 3.

4. Simulations and results

The deformation is investigated applying different applied cycle- and rest times and with different ballast shapes. The effect on the computational cost using the different ballast types, and computational relevant parameters are stated in Table 4. The tests are stated below.

- Variation in shape (test 1). Involves simulations of the different ballast models.
- Rest time variation (test 2). The rest time variation is an examination of the influence of the rest time. Rest time represents the interval of time between the load cycles.
- Cycle time variation (test 3). The cycle time represents the period of time in which one load cycle is simulated. The test is described in Appendix A.

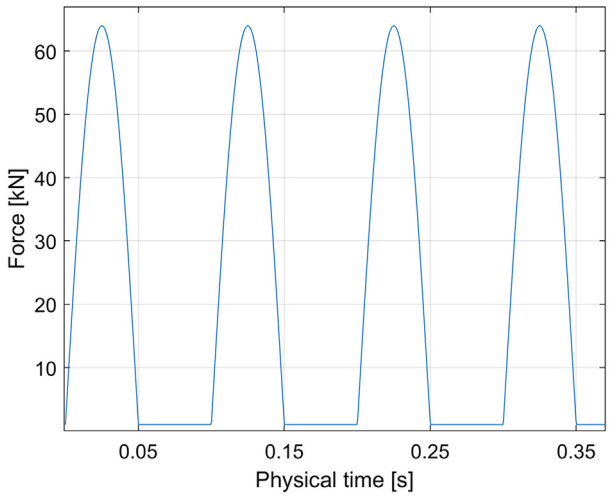

Fig. 5. Specified contact force. A 0.05 s of load and rest time, peak 63 kN trough 1 kN.

- A total of 13 simulations are presented and described in this study. The configurations of each simulation are presented in Table 5.

4.1. Variation in shape (test 1)

Four studies (Sim 1.1, 1.2, 1.3, and 1.4) are conducted to test the deformation on the different ballast models. The simulations are performed until they reach a constant rate of deformation per cycle. The results are presented by visualizing the computational domain before and after loading, and a plot of the applied force and associated deformation. Lastly the deformation in time is compared for all types of ballast as the same physical time corresponds to the same amount of cycles.

Table 4
Computational cost parameters.

Ballast type	Spheres	3D-scanned stones	Clumps
Particle count	11,182	13,276	65,199
Minimum diameter [cm]	4.00	0.87	1.69
Mean diameter [cm]	4.00	1.10	2.16
Minimum DEM time step [s]	4.43×10^{-6}	9.64×10^{-7}	1.88×10^{-6}
Mean DEM time step [s]	4.43×10^{-6}	1.22×10^{-6}	2.40×10^{-6}
*Computation time [s^{-1}]	4.3	12.6	65.9

* Computational time: duration (hours) used to simulate 1 s of physical time on an Xeon Gold 6148 processor running at 2.40 GHz.

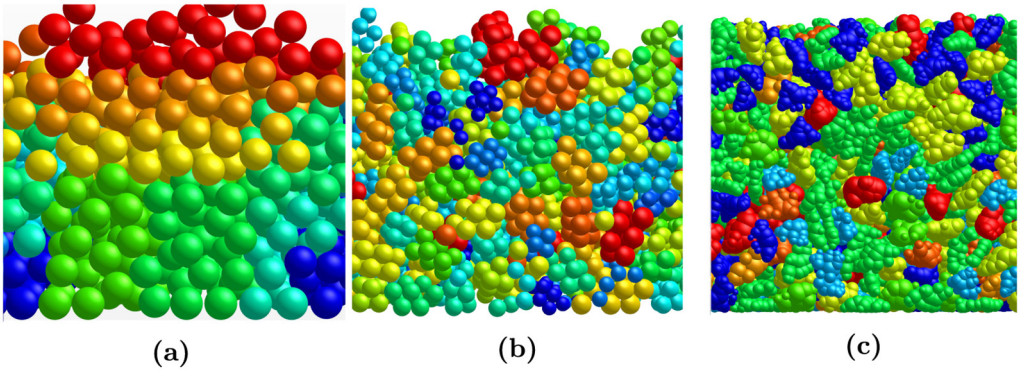

Fig. 4. Section view of the ballast models injected in the computation domain: (a) Spheres: ballast model 1 and 2; (b) Clumps: ballast model 3; (c) Stones: ballast model 4.

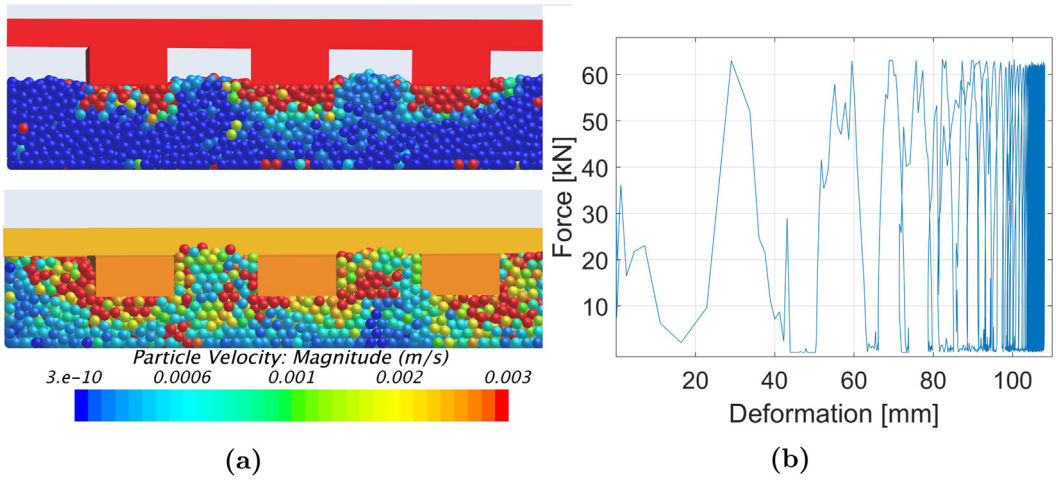

Fig. 6. Vertical deformation of spheres without rolling resistance (Sim 1.1). (a) Vertical deformation before and after loading. (b) Loading and vertical deformation plot. The sleepers, rails and ballast are colored by their velocity.

4.1.1. Spheres without rolling resistance (ballast model 1)

The spheres modelled without rolling resistance are simulated in a total of 80 load cycles (Sim. 1.1). The deformation of the track ballast is displayed in Fig. 6. The initial state shown in Fig. 6a displays sleepers that are partly submerged in the track ballast. This is caused by the weight of the sleepers and rails induced by gravity. After loading it is noted that the sleepers are fully submerged in the track ballast due to large ballast deformation. More than half of the total deformation occurs within the first 3 cycles cf. Fig. 6b. After 20 load cycles the sleepers are fully submerged at 108 mm, which is a poor representation of the reality.

4.1.2. Spheres with rolling resistance (ballast model 2)

The spheres modelled with rolling resistance are simulated at a total of 310 load cycles (Sim 1.2). The deformation is shown in Fig. 7. Before loading (Fig. 7a) the sleepers are positioned at different levels depending on the track ballast. After loading the sleepers are at the same height, and the sleepers are semi-submerged in the track ballast. The maximum obtained deformation is 58 mm. It is noted that the ballast is still deforming after 310 load cycles.

4.1.3. Clumps (ballast model 3)

The clumps are simulated at a total of 74 load cycles (Sim 1.3). From Fig. 8 it is observed that the sleepers are positioned in different heights similar to the spheres with rolling resistance. After loading the sleepers are placed at the same level. The total deformation is 27 mm as shown in Fig. 8. Within the first 5 load cycles a deformation of 19 mm is obtained. Ballast model 3 allows the bonds to break and 38 bonds are found to break during the simulation. In the simulation the number of broken bonds are decreasing over time, all 38 bonds are broken within the first 10 load cycles.

4.1.4. 3D-scanned stones (ballast model 4)

The 3D-scanned stones are simulated at a total of 122 load cycles (Sim 1.4). In Fig. 9a the computation section is shown. Before loading small cavities occurs underneath the sleepers. After loading the cavities are gone and the ballast has risen. The achieved total deformation is 14 mm. Within the first 5 load cycles a deformation of 6 mm is obtained.

4.1.5. Comparison of ballast models

The different ballast models are compared based on their level of deformation in Fig. 10. The ballast types are evaluated on the

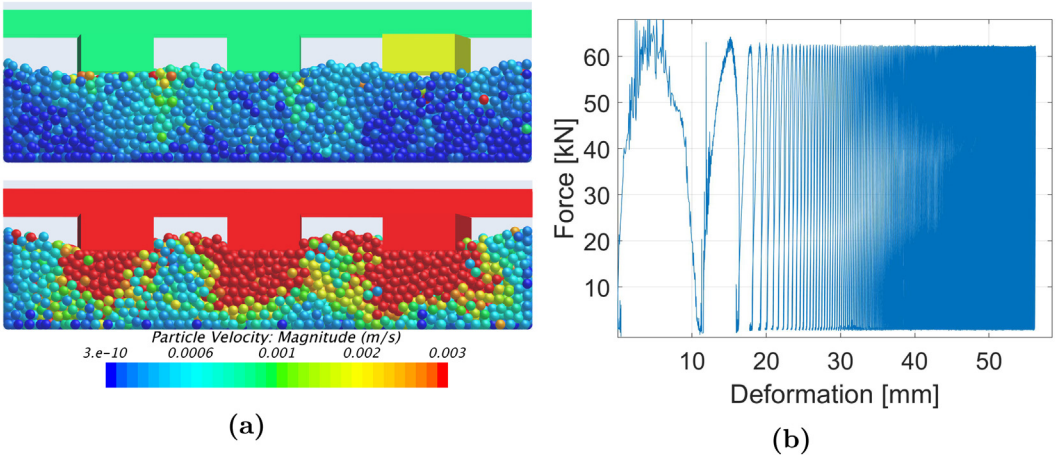

Fig. 7. Vertical deformation of spheres with rolling resistance (Sim 1.2). (a) Vertical deformation before and after loading. (b) Loading and vertical deformation plot. The sleepers, rails and ballast are colored by their velocity.

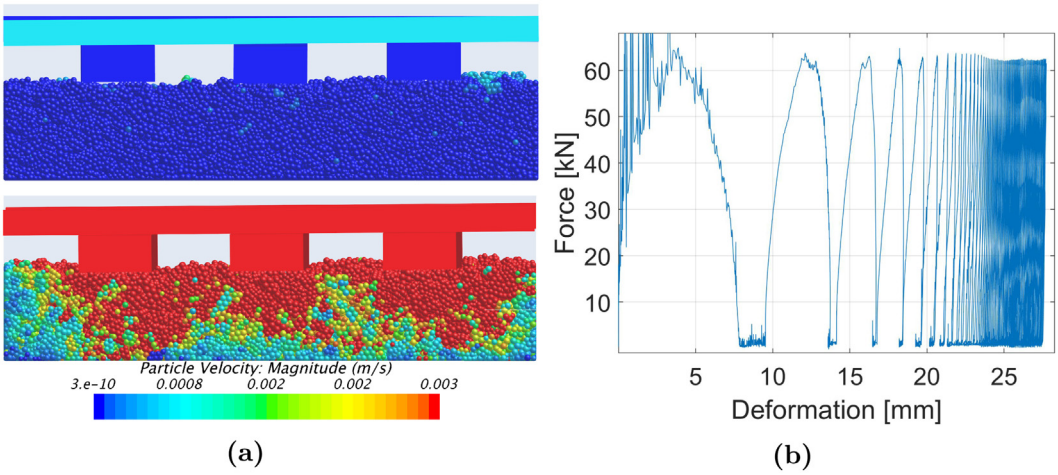

Fig. 8. Vertical deformation of clumps (Sim 1.3). (a) Vertical deformation before and after loading, (b) Loading and vertical deformation plot. The sleepers, rails and ballast are colored by their velocity.

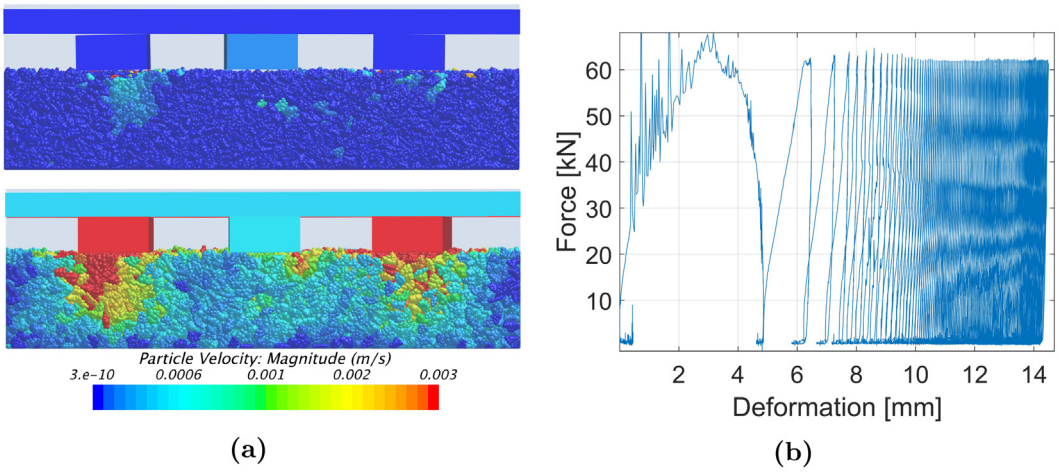

Fig. 9. Vertical deformation of stones (Sim 1.4). (a) Vertical deformation before and after loading. (b) Loading and vertical deformation plot. The sleepers, rails and ballast are colored by their velocity.

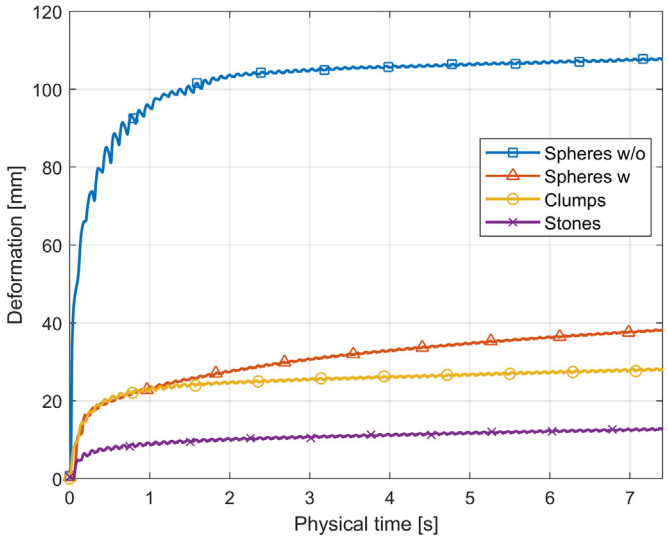

Fig. 10. Obtained deformation as function of physical time, for the different proposed ballast models (Sim 1.1, Sim 1.2, Sim 1.3, and Sim 1.4).

deformation of the first 7 s. Within 1 s of simulated time 10 load cycles occur. In general the ballast modelled as spheres reaches a higher level of deformation than the clumped particles (stones and clumps) within the same number of load cycles. The largest amount of deformation occurs within the first cycles. After the first cycles the ballast reaches a state in which the rate of deformation decreases drastically. This state is taken as an indicator of when the sleepers are settled in the ballast. The noteworthy difference between the spheres and the more complex shaped ballast (stones and clumps) is the interlocking potential of the complex shapes. The complex shapes has the opportunity to "lock" because of the non-spherical geometry, which the results justify, the complex shapes reaches stability before the rails reach the ballast. Track ballast modelled as spheres will deform until the rails reach the track ballast. With spheres it is not possible to simulate the interlocking potential of real stones, which is only achievable with non-spherical shapes.

4.2. Rest time variation (test 2)

In this section the importance of the rest period between each cycle is investigated. In a real life situation the rest period differs with the car length, train speed and wheel spacing. Four different rest times between

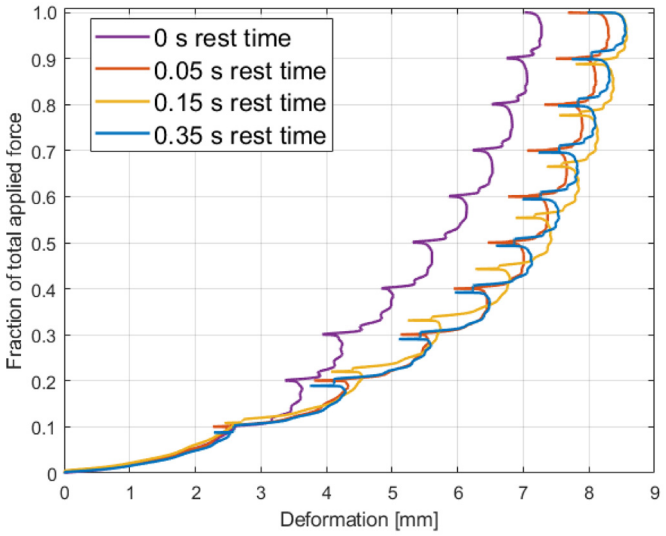

Fig. 11. Obtained deformation at different rest times: 0.00 s, 0.05 s, 0.15 s, and 0.35 s (Sim 2.1, Sim 2.2, Sim 2.3, and Sim 2.4).

the cycles are tested over 10 cyclic loads using the clumps model (ballast model 3). The simulations are all generated from the same injection to avoid other factors than the rest time to have an impact on the simulation results. The tested rest times are 0.00 s, 0.05 s, 0.15 s, and 0.35 s meaning the period of time simulated before the next cyclic load is applied. In Fig. 11, a significant difference between having no rest time and having rest time is observed. In Fig. 12 a load applied at time 1.65 s can be seen. The load stops at time 1.70 s and is followed by 0.35 s of rest time. At 1.75 s the deformation has almost stopped and after 1.80 s the deformation is considered stopped for the ballast. Fig. 11 shows the difference between different levels of rest time. Increasing the rest time from 0.00 s to 0.05 s doubles the computational cost. From 0.00 s to 0.15 s the computational cost quadruples while from 0.00 s to 0.35 s makes it eight times as computational expensive for the same amount of cycles. From the results it is also observed that the damping response is rather constant. Stability is regained in the same amount of time, independent of the number of load cycles applied, even tough greater deformations are observed in the initial load cycles. A rest-time of 0.05 s is chosen for the simulations in this study, since the impact on the deformation of having 0.15 s or 0.35 s of rest time compared to having 0.05 s s is relatively small.

A lower value of the restitution coefficient would possibly have lowered the computational cost. However the effect of this is not tested in this study.

Table 5
Table showing the simulation configurations of all tests conducted in the present study.

Simulation	Ballast model	Cycle time [s]	Rest time [s]
Test 1.	**Shape**		
Sim 1.1	Spheres	5×10^{-2}	5.0×10^{-2}
Sim 1.2	Spheres (Roll)	5×10^{-2}	5.0×10^{-2}
Sim 1.3	Clumps	5×10^{-2}	5.0×10^{-2}
Sim 1.4	3D-scan	5×10^{-2}	5.0×10^{-2}
Test 2.	**Rest time**		
Sim 2.1	Clumps	5×10^{-2}	0.0
Sim 2.2	Clumps	5×10^{-2}	5.0×10^{-2}
Sim 2.3	Clumps	5×10^{-2}	1.5×10^{-1}
Sim 2.4	Clumps	5×10^{-2}	3.5×10^{-1}
Test 3.	**Cycle time**		
Sim 3.1	Clumps	5×10^{-1}	5.0×10^{-1}
Sim 3.2	Clumps	5×10^{-2}	5.0×10^{-2}
Sim 3.3	Clumps	5×10^{-3}	5.0×10^{-3}
Sim 3.4	Clumps	5×10^{-4}	5.0×10^{-4}
Sim 3.5	Clumps	5×10^{-5}	5.0×10^{-5}

5. Conclusion and discussion

Track ballast has been studied during cyclic loading using the Discrete Element Method (DEM). The ballast was modelled polyhedrally, by fitting overlapping spheres into 3D scannings of real ballast stones. A thorough comparison study was conducted, comparing the ballast modelled by real ballast stones, with simplified ballast models commonly investigated in the literature. Furthermore more an innovative way of computing the sleepers was tested. The sleepers were injected in to the computational domain as polyhedral DEM particles, yielding an accurate representation of the degrees of freedom in the system. In addition the influence of the applied cycle- and rest time on the obtained deformation was studied. In relation to the present study the following conclusions are drawn,

- Modelling the track ballast from 3D-scanned ballast stones, along with representing the sleepers as DEM particles, is feasible and realistic results are obtainable.
- From the comparison of the 3D-scanned ballast method and the other proposed ballast models, the smallest deformation was obtained in ballast modelled from the 3D-scanning. The shape of the ballast has a significant influence on the solution, making this an important feature for predicting the ballast deformation. The main finding on this experiment was regarding the concept of interlocking. Interlocking can not be simulated on ballast modelled as spheres. Thus, aggregate shapes are needed to obtain realistic simulations.
- The influence of the cycle and rest time, here presented as trigonometric functions, was found to have a remarkable influence on the results of the simulations. The load curve depends on the train speed and car length.

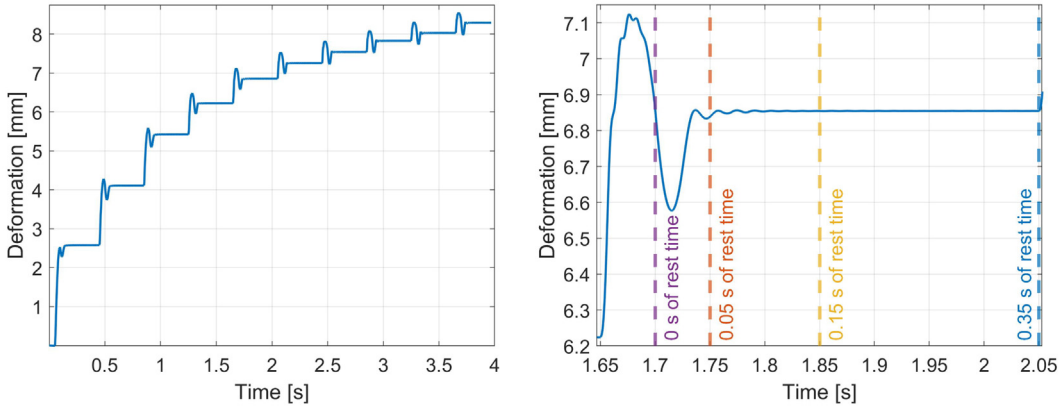

Fig. 12. Deformation over time using 0.35 s of rest time for 10 cycles. (a) Deformation for 10 cycles each followed by 0.35 s of rest time. (b) Zoom in at the load applied at time 1.65 s to 1.7 s followed by 0.35 s of rest time seen with the considered rest times.

The simulations showed great impacts on the obtained deformation, as well as the computational cost. For this reason, the loading profile is an important feature to refine in order to obtain reasonable results.

In the majority of similar studies the sleepers have been simulated as walls moving with a prescribed velocity, whereas the sleepers were modelled as DEM particles in this study, with a prescribed load. Furthermore the main deviations of the two types of sleeper modelling is that the DEM sleeper method is less rigid, and that it allows for axial sleeper rotations.

Declaration of Competing Interest

The authors declare that they have no known competing financial interests or personal relationships that could have appeared to influence the work reported in this paper.

Acknowledgements

The authors wish to thank Klaus Liltorp for technical advice regarding the use of the 3Shape D800 3D-scanner, and Nina Schou Kristensen from Banedanmark who provided the ballast stones for the research. Lastly, a thanks to DTU Compute for providing the necessary computer resources required for the study.

Appendix A. Impact of the applied cycle time

To investigate the influence of the cycle time on the ballast deformation five different cycle times are studied (test 3). The tests are performed using clumps (the ballast model 3), with the settings described in Table 5. The load-functions are evaluated on the fraction of applied force and the permanent vertical deformation of the ballast is shown in Fig. A.1. The influence of the cycle time is evaluated on the first 5 load-cycles. As seen 5×10^{-3} s, 5×10^{-4} s, and 5×10^{-5} s do not give satisfying deformation nor load-cycles similar to 5×10^{-1} s and 5×10^{-2} s. This is due to the fact that the contact forces do not reach the predefined force of 63 kN. Cycle times in the range of 5×10^{-3} s to 5×10^{-5} s is concluded to be unrealistic for this setup. Within the realistic range from 5×10^{-1} s to 5×10^{-2} s, it tends that shorter cycle times results in larger deformation for each load-cycle. It is observed that different cycle times leads to a significant difference in the deformation. In practical application the deformation tends to be larger at higher train velocities. Due to high computationally costs 5×10^{-1} s will not be further investigated (62.5 computation-hours/cycle at Intel Xeon 40). The cycle time of 5×10^{-2} s is concluded as a fair level of cycle time and is chosen for the simulations investigating the shape (test 1).

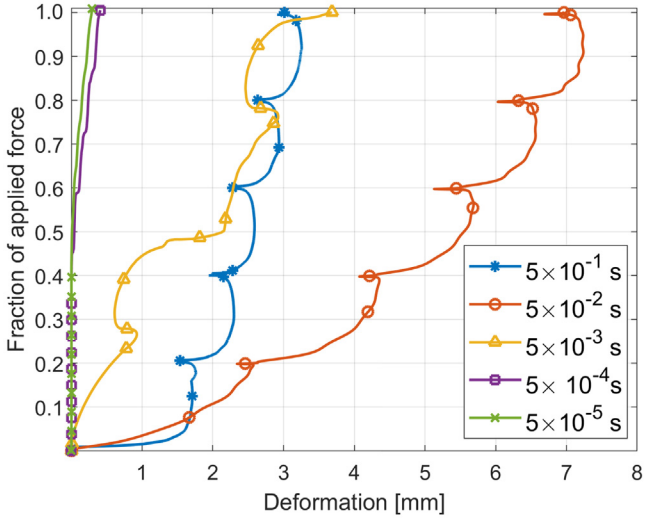

Fig. A.1. Sleeper deformation at the 5 different cycle times: (Sim 3.1, 3.2, 3.3, 3.4, and 3.5).

References

[1] E. Kassa, J.C.O. Nielsen, Stochastic analysis of dynamic interaction between train and railway turnout, Veh. Syst. Dyn. 46 (5) (2008) 429–449.
[2] P. Wang, J. Xu, K. Xie, R. Chen, Numerical simulation of rail profiles evolution in the switch panel of a railway turnout, Wear 366 (2016) 105–115.
[3] U. Olofsson, T. Telliskivi, Wear, plastic deformation and friction of two rail steels—a full-scale test and a laboratory study, Wear 254 (2003) 80–93.
[4] P.A. Cundall, O.D.L. Strack, A discrete numerical model for granular assemblies, Géotech 29 (1979) 47–65.
[5] A. Di Renzo, F.P. Di Maio, Comparison of contact-force models for the simulation of collisions in DEM-based granular flow codes, Chem. Eng. Sci. 59 (3) (2004) 525–541.
[6] D.O. Potyondy, P.A. Cundall, A bonded-particle model for rock, Int. J. Rock Mech. Min. Sci. 41 (2004) 1329–1364.
[7] S. Lobo-Guerrero, L.E. Vallejo, Discrete element method analysis of railtrack ballast during cyclic loading, Granul. Matter 8 (2006) 195–204.
[8] E. Mahmoud, A.T. Papagiannakis, D. Renteria, Discrete element analysis of railway ballast under cycling loading, Advances in Transportation Geotechnics III, Vol. 143 of Procedia Engineering 2016, pp. 1068–1076.
[9] P.J. Jensen, Sporteknik, Banedanmark Teknik, LCC Spor, 2017.
[10] H. Feng, Z. Jiang, F. Xie, P. Yang, J. Shi, L. Chen, Automatic fastener classification and defect detection in vision-based railway inspection systems, IEEE Trans. Instrum. Meas. 63 (4) (2014) 877–888.
[11] M.J.G. Romero, J.R. Edwards, C.P.L. Barkan, B. Wilson, J. Mediavilla, Advancements in fastening system design for North American concrete crossties in heavy-haul service, AREMA Annual Conference & Exposition, 2010.
[12] J.-A. Zakeri, F.H. Rezvani, Failures of railway concrete sleepers during service life, Int. J. Constr. Engng. & Manag. 1 (1) (2012) 1–5.
[13] R. Ford, Differential ballast settlement, and consequent undulations in track, caused by vehicle-track interaction, Veh. Syst. Dyn. 24 (sup1) (1995) 222–233.
[14] M.J. Shenton, Ballast Deformation and Track Deterioration, 1985 253–265, https://doi.org/10.1680/tt.02289.0026.
[15] M. Ishida, A. Namura, T. Suzuki, Track dynamic analysis for track settlement & irregularity growth, Proc. Int. Conf. Railway Engng, 2002 , (London, UK, July 2002, 2002).
[16] Y. Sato, Japanese studies on deterioration of ballasted track, Veh. Syst. Dyn. 24 (sup1) (1995) 197–208.
[17] E. Tutumluer, Y.M.A. Hashash, J. Ghaboussi, Y. Qian, S.J. Lee, H. Huang, Discrete Element Modeling of Railroad Ballast Behavior, Technical Report, University of Illinois Urbana-Champaign, USA, July 2018.
[18] B. Dahal, D. Mishra, Discrete element modeling of permanent deformation accumulation in railroad ballast considering particle breakage, Front. Built Environ. 5 (145) (2020) https://doi.org/10.3389/fbuil.2019.00145.
[19] T. Zhou, B. Hu, J. Sun, Z. Liu, Discrete element method simulation of railway ballast compactness during tamping process, Open Electrical Electronic Eng. J. 7 (2013) 103–109.
[20] J.H. Walther, I.F. Sbalzarini, Large-scale parallel discrete element simulations of granular flow, Eng. Comput. 26 (6) (2009) 688–697.
[21] L.E. Silbert, G.S. Grest, S. Plimpton, Boundary effects and self-organization in dense granular flows, Phys. Fluids 14 (2002) 2637–2646.
[22] Siemens, Simcenter STAR-CCM+ Documentation Version 2019.1, Siemens Simcenter, 2019.
[23] A. Al-Jawadi, Some Useful Numbers on the Engineering Properties of Materials, 615, GEOL, 2021.
[24] B. Sundström, Handbook of Solid Mechanics, Department of Solid Mechanics KTH, 2010.
[25] B. Suhr, W.A. Skipper, R. Lewis, K. Six, Shape analysis of railway ballast stones: curvature-based calculation of particle angularity, Sci. Rep. 10 (1) (2020) 6045.